ELSEVIER

Applied Surface Science 125 (1998) 227–235

applied surface science

Dynamics of laser produced silver plasma under film deposition conditions studied using optical emission spectroscopy

Riju C. Issac *, K. Vasudevan Pillai, S.S. Harilal, Geetha K. Varier, C.V. Bindhu, Pramod Gopinath, P. Radhakrishnan, V.P.N. Nampoori, C.P.G. Vallabhan

Laser Division, International School of Photonics, Cochin University of Science and Technology, Cochin 682 022, India

Received 14 May 1997; accepted 13 September 1997

Abstract

Laser produced plasma from silver is generated using a Q-switched Nd:YAG laser. Optical emission spectroscopy is used to carry out time of flight (TOF) analysis of atomic particles. An anomalous double peak profile in the TOF distribution is observed at low pressure. A collection of slower species emerge at reduced pressure below 4×10^{-3} mbar and this species has a greater velocity spread. At high pressure the plasma expansion follows the shockwave model with cylindrical symmetry whereas at reduced pressure it shows unsteady adiabatic expansion (UAE). During UAE the species show a parabolic increases in the expansion time with radial distance whereas during shock wave expansion the exponent is less than one. The angular distribution of the ablated species in the plume is obtained from the measurement of optical density of thin films deposited on to glass substrates kept perpendicular to the plume. There is a sharp variation in the film thickness away from the film centre due to asymmetries in the plume. © 1998 Elsevier Science B.V.

PACS: 52.59.Jm; 52.25.Ya; 52.25.Rv

Keywords: Laser produced plasma; Time of flight measurements; Emission spectroscopy

1. Introduction

Pulsed laser deposition (PLD) of various materials is effectively being used for thin film preparation during the past few decades [1,2]. It has been proved to be a convenient and accurate method for thin film deposition as better control over film characteristics can be obtained by varying the laser parameters and ambient conditions. PLD of high-Z metallic multilayer superlattices are employed in the development of X-ray mirrors [3]. Metal buffer layers are said to be useful for the deposition of high T_c superconducting thin films [4]. Because of the low resistivity and stability, thin metal films are widely used in optoelectronics and integrated circuits for forming ohmic contacts with semiconductors. However, the full utilization of laser ablation in single element thin film deposition has not been possible due to various reasons [3,9]. The successful deposition of stoichiometric thin films by the method of PLD demands the characterization of the ablation plume with temporal, spatial and angular resolutions [5–10]. Another motivation for the laser ablation of pure metals is to understand the basic plasma kinetics as well as for

* Corresponding author. E-mail: root@cochin.ernet.in.

PII S0169-4332(97)00415-7

producing highly ionized hydrogen-like and helium like ions [11–13].

The various phenomena like laser plasma interactions [14], cluster formation and dissociation [15–17], gas phase chemical reactions [18,19], plasma ionization [16], etc., make it rather difficult to understand the evolution and dynamics of laser produced plasma completely. In spite of all these variety of primary and secondary mechanisms, laser ablation of solids have been the subject of extensive research in recent times [20–22]. Mechanisms of laser ablation varies widely with the mechanical, thermal and absorptive properties of the material as well as the laser parameters and ambient conditions [23,24]. There are a number of research articles describing the dynamics of the plasma plume with respect to ambient pressure, laser power density, laser wavelength, etc. [25–29]. In spite of the extensive theoretical and experimental investigations carried out till date, the laser beam interaction with material, the evolution of the plasma, the gas phase dynamics and the conditions for congruent material transfer towards the substrate are not completely known. The presence of an ambient gas, for example, alters the properties of the plume significantly [30,31]. At high ambient pressure the plasma plume has a large angular spread due to scattering but in vacuum this scattering is negligible. Geohegan and Purezky [32] describe the broadening of the time of flight (TOF) profile in yttrium plasma at high pressure levels due to collisions with the background gas molecules. In vacuum, they found a narrow velocity profile for ionic species. Their observations have also revealed a fast and a slow component at high ambient pressure while only the fast component persists in vacuum. The slower component actually emerge due to the slowing down of the plume by ambient gas molecules. Such double peak structure appears only for limited distances and pressures.

Gas phase collisions inside the plasma play a major role in determining the spatial, temporal and angular distribution of ablated species. When the particle densities are high enough, collisions induce the formation of a thermalization layer called Knudsen layer (KL) within a few mean free paths from the target surface. Investigations on the formation of such a layer in laser produced plasmas have been done by Kelly et al. and others [33–38]. The formation of the KL results in stopped or backward moving material close to the target and strongly forward peaked velocity distributions away from the target. The 'half range' Maxwellian velocity distribution is changed over to a 'full range' Maxwellian distribution revealing the presence of backward moving particles. The backward moving particles are either recondensed or reflected from the target surface. The KL formation is followed by a more forward peaked particle flux with an unsteady adiabatic expansion (UAE) of the plasma.

In the present paper some aspects of the dynamics of laser ablated silver plasma in an argon ambient is studied. Argon gas is chosen since the presence of the inert ambient gas will reduce the possibility of gas phase reactions and formation of molecules. The silver plasma becomes a favourite choice because of its monocomponent nature which is suited for studying laser–target, laser–plasma interactions and gas phase kinetics. Silver metal films are used for the fabrication of good quality ohmic contacts to semiconductors as well.

2. Experimental details

The experimental configuration adopted for TOF measurements is schematically shown in Fig. 1. The plasma is produced using a Q-switched Nd:YAG laser (Quanta Ray, DCR 11) operated at the fundamental wavelength of 1.064 μm with pulse width 10 ns and repetition rate 10 Hz. The target is a disk of silver having diameter 1.5 cm and thickness 1 mm which is kept inside a plasma chamber and is rotated in order to avoid multiple hits at the same location for long time. A convex lens of focal length 30 cm focuses the laser beam to the target (spot radius 50 μm). Laser beam hits the target surface at an angle of 45° for film deposition and at 90° during TOF studies. The chamber is connected to diffusion and rotary vacuum pumps and an ultimate pressure of 10^{-5} mbar is obtained in the system. The chamber also has glass windows for optical monitoring and provisions for thin film substrate holders. The TOF measurements were done after one-to-one imaging of the luminous plasma plume on to the entrance slit of a monochromator by appropriate collimating and focusing lenses. Using proper slits and apertures any

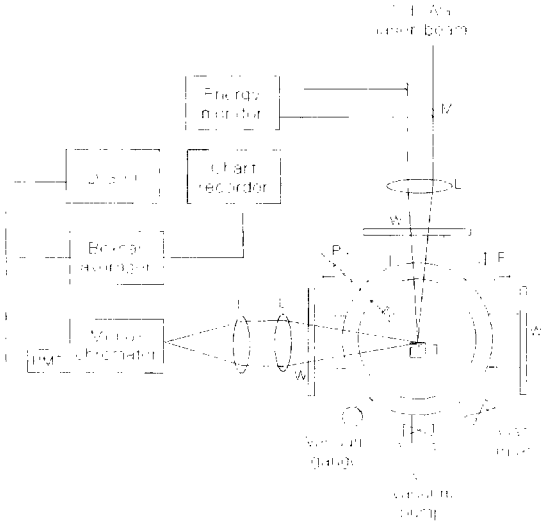

Fig. 1. Block diagram of the experimental setup. M: 10% reflector, L: lens, W: glass windows, P: substrate insertion port, T: rotating target holder, PMT: photomultiplier tube, DSO: digital storage oscilloscope. The laser spot size was 50 μm in radius.

vertical segment of the plasma situated at definite distances from the target surface can be selected for analysis. The wavelength selection was done by a high resolution spectrometer (SPEX Model 1704, 1 m, grating with 1200 grooves per mm blazed at 5000 Å and slit width limited resolution 0.15 Å). A thermoelectrically cooled photomultiplier tube (Thorn EMI, KQB-9683) was used as the photodetector at the exit slit of the monochromator. The time of flight signals are monitored on a digital storage oscilloscope (500 MHz, Hewlett Packard, HP 54610). The laser pulse energy is measured with a calibrated laser energy meter (Delta Developments) and the power density at the focal spot is calculated after reflection corrections from the lens and window surfaces.

3. Results and discussion

The Nd:YAG laser output is focused on to the silver target and the laser ablated plasma is produced in vacuum using an irradiance level of 5×10^{10} W cm^{-2}. A luminous plasma appears in front of the target with ejected particle velocities of the order of 10^6 cm s^{-1}. The optical emission spectrum in the region $\lambda = 3500$–6000 Å is monitored and emission lines from various atomic and ionic species are identified. Among the various emission lines, atomic lines of silver are most dominant. A few lines from singly ionized silver and argon are also present with reduced intensities. The monochromator is set at a fairly intense emission line of atomic silver (viz. 5465 Å) and its intensities are monitored at various spatial distances away from the target surface. The TOF signals are investigated as a function of both the background gas pressure and distance away from the target surface.

3.1. Time of flight measurements

Optical probing of particle evolution is a well accepted method for the study of laser generated plasma as has been demonstrated by several workers [16,17,39–41]. Fig. 2 show the oscilloscope traces of the TOF signal of atomic silver at a laser power density of 5×10^{10} W cm^{-2} at various ambient pressures and at a distance of 0.5 cm in front of the target surface. As has been reported earlier for the case of ionic species [41], one may expect the velocity to increase as the pressure is decreased since the collisional deceleration and scattering of the particles with the ambient gas molecules is much lower at reduced pressures. Also the TOF signal became narrower implying lower velocity spread as the pressure is lowered. However, in the present studies, at ambient pressures below 4×10^{-3} mbar a second peak is

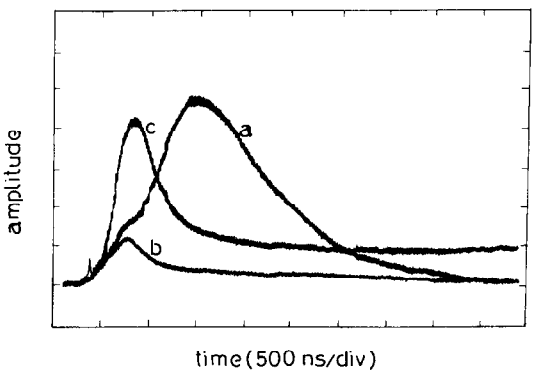

Fig. 2. Time of flight profile at different ambient pressures: (a) 2×10^{-5} mbar, (b) 0.09 mbar, and (c) 0.37 mbar. The optical emission lineat 5465 Å from excited silver atoms is selected for temporal measurements. The data is taken 0.5 cm from the target and at a laser power density 5×10^{10} W cm^{-2}.

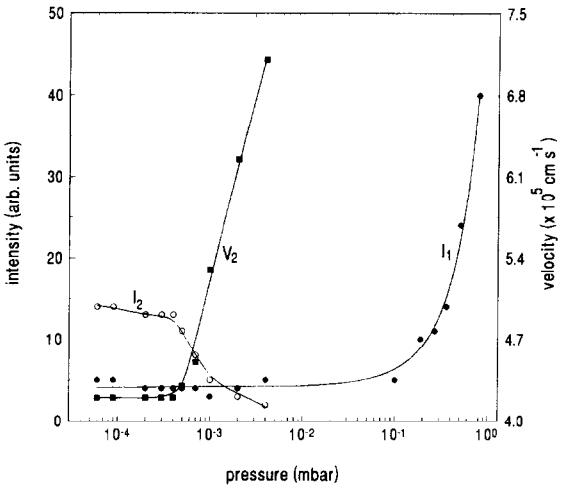

Fig. 3. Intensity and velocity of the two peaks with respect to chamber pressure. There exists an intermediate pressure region where the plasma emission is almost nil.

developed in the TOF signal indicating a slower component. The temporal spread is larger for the newly developed peak and a trace of a fast component also is seen. The two sets of atomic species in the plasma seem to possess independent dynamics as will be seen below.

Fig. 3 shows the intensities as well as the velocities of the two peaks (hereafter we use the notation P1 for the faster peak and P2 for the delayed peak developed at low pressure) as a function of ambient pressure. The emission intensity not only corresponds to the overall plume density but also the plasma temperature. The fast component, P1 has maximum intensity at relatively high ambient pressures and the intensity gradually reduces as the pressure is reduced. This can be attributed to the populated excited states due to various collisional processes like three body recombination of ions and electrons, electron impact excitation etc. which in turn depend on the temperature as well as the density of the plasma which decide the charge transfer and recombination processes. However, the intensity of P2 is developed below 4×10^{-3} mbar and is almost constant below 1×10^{-3} mbar. Therefore, an additional excitation source for the neutrals is indicated below 4×10^{-3} mbar. The velocity (V_2) of the species corresponding to the P2 is found to increase with the pressure till the two peaks merge with each other above 10^{-2} mbar. This shows that initially at relatively high pressure the two types of species have the same dynamics. The peak velocity corresponding to P2 has a constant value of 1.7×10^6 cm s^{-1} (not shown in the figure) at different pressures and within the plasma boundary with the ambient gas. That is, P2 is unaffected by the presence of the background gas. This component is the one which penetrates the background gas with almost the same velocity as in the case velocity in vacuum. The decrease in intensity could be due to the depletion of the excited state molecules at reduced pressure due to smaller number of collisional excitations.

3.2. Spatial measurements

The intensity as well as the velocity at a pressure of 2×10^{-5} mbar as a function of distance from the target is shown in Fig. 4. The intensity of P1 is rapidly decreased just above the target surface and thereafter it levels off. But in the case of the P2 at reduced pressure, the intensity first shows a small increase and then gradually decreases. Therefore, one can safely assume that the major source of the slower species is not the target surface, but they originate from a region slightly away from the target surface. The intensity maximum occurs at a distance of about 0.1 cm away from the target surface. The velocities at various distances are also shown in Fig.

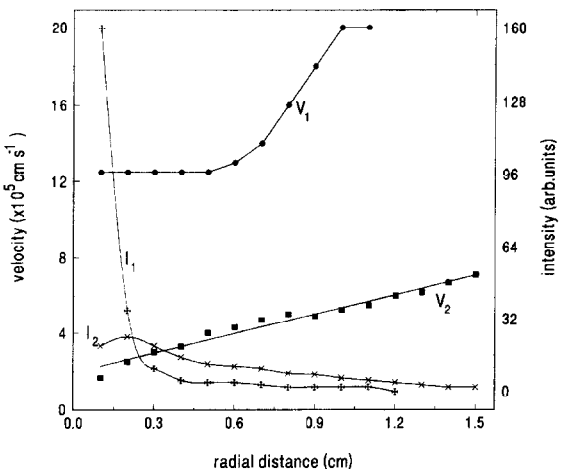

Fig. 4. Variation of the intensities and peak velocities of the two set of silver atoms with respect to distance from the target at 2×10^{-5} mbar.

4. For P1, the velocity remains steady up to about 0.6 cm and there after increases linearly. This means that above a certain distance, the particles obtain an additional kinetic energy. One possible reason for this could be the three body recombination of ions and electrons. The energy gained through three body recombination is converted to kinetic energy of atoms. Recombination is more probable in regions where plasma temperature is low, i.e., away from the target. The linear increase in the velocity is in agreement with the widely accepted theory of adiabatic plasma expansion [28,29]. During adiabatic expansion, the x-component of the velocity v_x is given by the relation

$$v_x = \frac{x}{X(t)} \frac{\mathrm{d}X(t)}{\mathrm{d}t}. \quad (1)$$

Here $X(t)$ is the dimension of the expanding plasma in x-direction and correspond to the distance at which the plasma density decreases to 60.65% [29]. In the case of adiabatic plasma expansion, the velocities of all the constituent species increase linearly with distance from the target. In the case of P2, the velocity shows a linear increase with distance, characteristic of adiabatic plasma expansion. These observations on the intensity and velocity variations with respect to pressure and distance from the target clearly reveal the independent origin and dynamics of these two species as mentioned earlier.

At relatively high pressures, the plasma has to encounter increased resistance from the ambient gas molecules and a shockwave is formed at the plasma boundary. In general, there are various models like the drag model and the shock model which satisfactorily describe the plasma dynamics in the presence of an ambient gas. Drag model predicts that the plume will come to rest as a result of the resistance due to collisions with the ambient gas. In the shock model the expanding products ejected from the target act like a piston which accelerate the ambient gas to supersonic speeds causing a shockwave ahead of the contact surface [42,43]. Within the assumptions pertaining to strong explosions, the position of the shock front R can be described as [43],

$$R \approx \xi \left[\frac{Et^2}{\rho(\infty)} \right]^n, \quad (2)$$

where ξ is a scaling factor (≈ 1 for air), $\rho(\infty)$ is the undisturbed density of background gas, E is given by the sum of the kinetic energy of the shockwave and the thermal energy of the vapor plume. The value of n depends on the symmetry of the shock front and for cylindrical symmetry $n = 1/4$ [43]. In our case at relatively high pressure only the fast peak appears and the position–time plot for this is shown in Fig. 5 at a pressure of 0.09 mbar. The dotted line is a power law fit to the data showing that the shock front obeys $R \propto \sqrt{t}$. This shows that the shockwave almost has a cylindrical symmetry. At low pressure both P1 and P2 do not give any indication of the formation of the shockwave but instead show a rapid increase in R with time. Parabolic fits of the observed data for P1 and P2 are shown in Fig. 5 corresponding to $n = 1$ in Eq. (2) and with different scaling factors ξ. Thus, such a behavior turns out to be characteristic of adiabatic expansion.

The velocity of the particle has a functional relationship of

$$v = aR^{-3(1-\alpha)}, \quad (3)$$

where a is a constant [42]. Here α is a fraction defined as $P_c = \alpha P$, where P_c is the pressure at the inner side of the shock front and P is the pressure

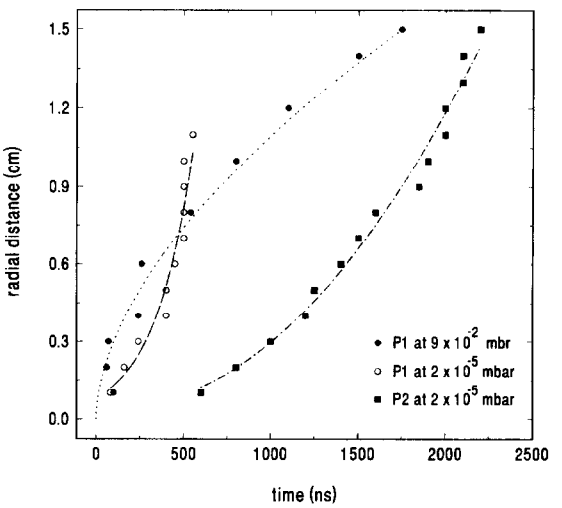

Fig. 5. Distance from the target (R) as a function of time (t). At relatively high pressure (0.09 mbar typically) the dependence is close to $R \propto \sqrt{t}$ while at reduced pressure the two peaks show much steeper evolution.

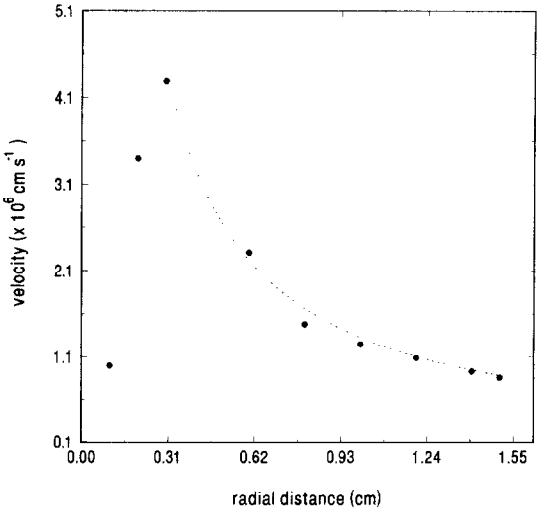

Fig. 6. Peak velocity corresponding to P1 as a function of radial distance at 0.09 mbar pressure. The dotted line represents a fit to the data satisfying the shock model of plasma expansion.

behind the shock front. Fig. 6 shows the velocity as a function of the radial distance above the target at 0.09 mbar. Initially the velocity shows a linear increase and it eventually comes down beyond a distance 0.3 cm from the target. The dotted line in the figure is a model fit to the observed data for distances greater than 0.3 cm with $\alpha = 2/3$ and $\alpha = 4/3$. At reduced pressure such a power law dependence of R on t such as the one described above is not observed.

3.3. Angular dependence of ablated species

When the minimum number of collisions is greater than three per particle KL is formed in a region within a few mean free paths from the target surface [33]. The exponential part of the velocity distribution changes from $\exp(-mv_x^2/2kT_s)$ to $\exp[-m(v_x - u_K)^2/2kT_K)$ where u_K is the positive flow velocity given by $u_K = (\gamma kT_K/m)^{1/2}$ [44]. Here m is the mass of the species, T_s is the surface temperature and T_K, the temperature of the species which is lower than T_s. Also the angular distribution is more forward peaked than those in the usual thermal sputtering. At these pressures compared to vacuum the collisions among the particles are more frequent and the KL is formed. The peak velocity is shifted to the higher side implying the existence of collisions as well as the formation of KL. Angular distributions of the ablated species are of interest during thin film deposition and is usually measured either by monitoring the ion flux using an electronic probe or from the thickness profile of the deposited film assuming a unity sticking coefficient to the substrate [8]. Here we followed the method used by Afonso et al. [45] where instead of measuring the thickness, the optical density is monitored as a function of the distance from the film center. The films are deposited on glass substrates (7.5×1.75 cm^{-2}) at room temperature and under various pressure conditions. The target is kept at 45° with the incident laser beam and the substrate was kept parallel to the target surface. The deposited film is partially transparent and electrically nonconducting. The optical density of the film as a function of the distance from the film center is measured using a microdensitometer. Fig. 7 shows the plot of optical density as a function of the distance from film center at a background pressure 0.09 mbar. Both the vertical and the horizontal distributions are measured and it is clear from the figure that both are essentially different from each other. The angular distribution is narrow along the horizontal direction and much broader in the vertical direction. Such elliptical isothickness behavior has been theoretically and experimentally demonstrated by

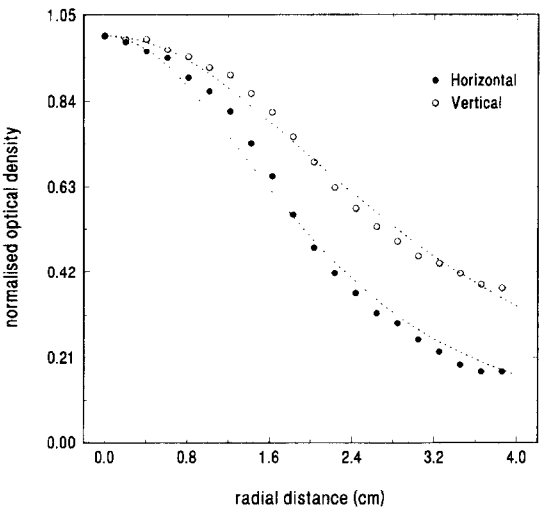

Fig. 7. Optical density as a function of distance from film center at a pressure of 0.09 mbar.

Singh and Narayan [28,29]. The species velocities will be maximum in the direction having smaller initial dimensions. Thus, the plasma becomes elongated in a direction having smallest initial dimensions. In the present case as well as in most of the laser deposition experiments, because of the 45° angle of incidence, the etch spot will be elliptical with major axis along the horizontal direction. Therefore, the particle velocity will be maximum along the vertical direction. An analytic expression for the film thickness distribution is given by [46]

$$D(x, 0, L) = \frac{D_0}{\left[(k_x x/L)^2 + 1\right]^{3/2}}, \quad (4)$$

where $D_0 = n_0 k_x k_y / 4\pi L^2$, $k_x = V_z/V_x$, $k_y = V_z/V_y$, V_a $(a = x, y, z)$ are the velocities in the three perpendicular axes, z being the propagation axis, n_0 is the total number of particles in the plasma and L the target–substrate distance. Similarly in the y-direction x and k_x are replaced by y and k_y in the above expression. The dotted lines in Fig. 7 show the theoretical fit to the data at 0.09 mbar for $k_x = 1.935$ for horizontal direction and $k_y = 1.315$ for the vertical. The values of k_x and k_y show that the vertical velocity is ≈ 1.46 times that of the horizontal. For 45° angle of incidence, the major axis is 1.414 times greater than the minor axis and according to the theory of adiabatic plasma expansion, the velocities also should have the same ratio [29]. The ratio $k_y/k_x \approx 1.46$ which is in close agreement with the value 1.414. In vacuum $k_x/k_y \approx 1.56$ deviating from the predicted value. Even though the dotted lines show a nearly close agreement with the data points in the vicinity of the film centre as well as at the wings, there exists an abrupt change in the thickness distribution in between. Near the film center the thickness is more uniform than predicted by Eq. (3) and beyond a certain distance the change is steeper. This means that there exists an emission solid angle inside which the particle flux is high and this region can be termed as the plasma core. The outer surface of the core is rarer and forms a halo. The deposition rate from the core is more than that from the halo. This is an indication that the energetic particles are more favorable for thin film growth.

One can see from Fig. 1 that the peak velocities of silver atoms decrease and the velocity spread (V_s) increases as the pressure goes down. Velocity spread is a clear demonstration of the randomness of particle motion. The ratio $V_s/V_p = \tan\theta$ gives the mean angle of particle emission [18]. The mean angle of particle emission, θ, is determined using the TOF signals at two pressures using the above formula and the values obtained are $\approx 35°$ at 0.09 mbar and $\approx 44°$ at 2×10^{-5} mbar. Accordingly the angular spread of the excited silver atoms is more at reduced pressure. Therefore, the angular spread of the ablated species as determined from film based methods significantly differs from the above data. Even though the neutrals in the plasma has an angular spread (FWHM) of 44°, the film based methods show that the spread 39° at 2×10^{-5} mbar. This suggests that excited neutral silver atoms are newly generated at reduced pressure and this has wide angular spread. One can consider that these are the reflected particles from the etch spot after backscattering from the Knudsen layer.

4. Conclusions

The TOF signal and angular distributions of ablated species are investigated as a function of Argon ambient pressure. An anomalous behavior in the temporal profile of silver atoms inside the plasma is observed. Above a pressure of 4×10^{-4} mbar, only one peak in the TOF profile exists while below that pressure a new peak begins to develop. The newly developed peak gives a maximum velocity for silver atoms which is much lower than that indicated by the first peak. The faster component expands one dimensionally with a constant velocity of 1.25×10^6 cm s^{-1} upto a distance ≈ 0.6 mm. Thereafter it expands adiabatically with a more forward peaked velocity distribution. This velocity does not appear to change with pressure. The peak due to low velocity components developed at reduced pressure shows the behavior of unsteady adiabatic expansion. The corresponding particles may be those which are retroreflected from the ablation spot. A detailed discussion of various aspects of retroreflected particles will be given elsewhere. There exists a boundary-like behavior in the thickness of the deposited film which again shows the directive nature of the ablated species.

This suggests that deposition rate depends critically on plasma parameters and reveals the effective role of the hot species inside plasma core. This velocity spread of the slow peak is an indication of the randomness in the velocities of the species. The dynamics of the two types of species is found to be entirely different from each other. At reduced pressure the KL feeds an unsteady adiabatic expansion with more forward peaked angular distribution. Spatio-temporal data at relatively high pressure show that the plasma can be modelled according to the predictions of shock wave theory of plasma expansion. The observed data show that the shockwave has cylindrical symmetry. But at reduced pressure this model does not fit with experimental data, obviously because there exist only negligible resistance and scattering from the surrounding gas molecules.

Acknowledgements

The present work is supported by the Department of Science and Technology, Government of India. The authors R.C.I. and C.V.B. are thankful to University Grants Commission (New Delhi) for their research fellowships and S.S.H. wishes to acknowledge Council of Scientific and Industrial Research (New Delhi) for a research fellowship.

References

[1] D.B. Chrisey, G.K. Hubler (Eds.), Pulsed Laser Deposition of Thin Films, Wiley, New York, 1994, and references therein.
[2] J.C. Miller, D.B. Geohegan (Eds.), Laser Ablation: Mechanisms and Applications – II, American Institute of Physics, New York, 1994.
[3] J.C.S. Kools, in: D.B. Chrisey, G.K. Hubler (Eds.), Pulsed Laser Deposition of Thin Films, Wiley, New York, 1994, p. 455.
[4] R.E. Russo, R.P. Reade, J.M. McMillan, B.L. Olsen, J. Appl. Phys. 68 (1990) 1354.
[5] D.B. Geohegan, Thin Solid Films 220 (1992) 138.
[6] J. Gonzalo, C.N. Afonso, F. Vega, D. Martinez Garcia, J. Perriere, Appl. Surf. Sci. 86 (1995) 40.
[7] T. Venkatesan, X.D. Wu, A. Inam, Y. Jeon, M. Croft, E.W. Chase, C.C. Chang, J.B. Watchman, R.W. Odom, F.R. di Brozolo, C.A. Magee, Appl. Phys. Lett. 53 (1988) 1431.
[8] K.L. Saegner, in: D.B. Chrisey, G.K. Hubler (Eds.), Pulsed Laser Deposition of Thin Films, Wiley, New York, 1994, p. 199.
[9] I. Weaver, C.L.S. Lewis, J. Appl. Phys. 79 (1996) 7216.
[10] P.E. Dyer, Appl. Phys. Lett. 55 (1989) 1630.
[11] Z. Andreic, V.H. Bartolic, H.J. Kunze, Phys. Scr. 48 (1993) 331.
[12] U. Teubner, T. Mirsala, I. Uschmann, E. Foster, W. Theobald, C. Wulkern, Appl. Phys. B 62 (1996) 213.
[13] W. Piestch, B. Dubreuil, A. Briand, Appl. Phys. B 61 (1995) 267.
[14] E.G. Gamaly, Lasers and Particle Beams 12 (1994) 185.
[15] R.W. Dreyfuse, J. Appl. Phys. 69 (1991) 1721.
[16] S.S. Harilal, R.C. Issac, C.V. Bindhu, V.P.N. Nampoori, C.P.G. Vallabhan, J. Appl. Phys. 80 (1996) 3561.
[17] S.S. Harilal, R.C. Issac, C.V. Bindhu, V.P.N. Nampoori, C.P.G. Vallabhan, J. Appl. Phys. 81 (1997) 3637.
[18] G. Hatem, C. Colon, J. Campose, Spectrochim. Acta A 49 (1993) 509.
[19] S.S. Harilal, R.C. Issac, C.V. Bindhu, G.K. Varier, V.P.N. Nampoori, C.P.G. Vallabhan, Pramana J. Phys. 46 (1996) 145.
[20] G.K. Varier, R.C. Issac, S.S. Harilal, C.V. Bindhu, V.P.N. Nampoori, C.P.G. Vallabhan, Spectrochim. Acta B 52 (1997) 657.
[21] R. Kelly, M. Miotello, in: D.B. Chrisey, G.K. Hubler (Eds.), Pulsed Laser Deposition of Thin Films, Wiley, New York, 1994, p. 55, and references therein.
[22] W. Piestch, J. Appl. Phys. 79 (1996) 1250.
[23] S.S. Harilal, R.C. Issac, C.V. Bindhu, V.P.N. Nampoori, C.P.G. Vallabhan, Jpn. J. Appl. Phys. 36 (1997) 134.
[24] G.J. Pert, J. Plasma Phys. 49 (1993) 295.
[25] W. Sesselmann, E.E. Marinero, T.J. Chuang, Appl. Phys. A 41 (1986) 209.
[26] A. Ritcher, Thin Solid Films 12 (1994) 185.
[27] Y. Lida, Spectrochim. Acta B 45 (1990) 1353.
[28] R.K. Singh, D.W. Holland, J. Narayan, J. Appl. Phys. 68 (1990) 233.
[29] R.K. Singh, J. Narayan, Phys. Rev. B 41 (1990) 8843.
[30] K. Scott, J.M. Huntley, W.A. Philips, J. Clarke, J.E. Field, Appl. Phys. Lett. 57 (1990) 922.
[31] P.E. Dyer, A. Issa, P.H. Key, Appl. Surf. Sci. 46 (1990) 89.
[32] D.B. Geohegan, X. Puretzky, Appl. Phys. Lett. 67 (1995) 197.
[33] R. Kelly, R.W. Dreyfuse, Surf. Sci. 198 (1988) 263.
[34] R. Kelly, D. Braren, Appl. Phys. B 160 (1991) 169.
[35] I. Noorbatcha, R.R. Luichase, Y. Zeire, J. Chem. Phys. 89 (1988) 5251.
[36] J.R. Ho, C.P. Grigoropolous, J.A.C. Humphry, J. Appl. Phys. 79 (1996) 7205.
[37] R. Kelly, R.W. Dreyfuse, Nucl. Instr. Meth. Phys. Res. B 32 (1988) 341.
[38] J.C.S. Kools, J. Appl. Phys. 74 (1993) 6401.
[39] D.B. Geohegan, in: D.B. Chrisey, G.K. Hubler (Eds.), Pulsed Laser Deposition of Thin Films, Wiley, New York, 1994, p. 115.

[40] W. Marine, M. Gerri, J.M. Scotto d'Aniello, M. Sentis, P. Delaporte, B. Forester, M. Fontaine, Appl. Surf. Sci. 54 (1992) 264.
[41] D.B. Geohegan, Appl. Phys. Lett. 60 (1992) 2732.
[42] Y.B. Zel'dovich, Y.P. Raizer, Physics of Shock Waves and High Temperature Hydrodynamic Phenomena, vol. I, Academic, New York, 1966.
[43] D. Baurle, Laser Processing and Chemistry, Springer-Verlag, Berlin, 1996, p. 533.
[44] R. Kelly, J. Chem. Phys. 92 (1990) 5407.
[45] C.N. Afonso, R. Serna, F. Catalina, D. Bermejo, Appl. Surf. Sci. 46 (1990) 249.
[46] F. Antoni, C. Fuchs, E. Fogarassy, Appl. Surf. Sci. 96–98 (1996) 50.